Predicting lithium iron oxysulphides for battery cathodes

Bonan Zhu[*,†,‡] and David O. Scanlon[*,†,¶,§,‡]

†*Department of Chemistry, University College London, 20 Gordon St, Bloomsbury, London WC1H 0AJ, United Kingdom*

‡*The Faraday Institution, Quad One, Becquerel Avenue, Harwell Campus, Didcot, OX11 0RA, United Kingdom*

¶*Thomas Young Centre, University College London, Gower Street, London WC1E 6BT, United Kingdom*

§*Diamond Light Source Ltd., Diamond House, Harwell Science and Innovation Campus, Didcot, Oxfordshire OX11 0DE, UK*

E-mail: bonan.zhu@ucl.ac.uk; d.scanlon@ucl.ac.uk

Abstract

Cathode materials that have high specific energies and low manufacturing costs are vital for the scaling up of lithium-ion batteries (LIBs) as energy storage solutions. Fe-based intercalation cathodes are highly attractive because of the low cost and the abundance of raw materials. However, existing Fe-based materials, such as $LiFePO_4$, suffer from low capacity due to the large size of the polyanions. Turning to mixed anion systems can be a promising strategy to achieve higher specific capacity. Recently, anti-perovskite structured oxysulphide Li_2FeSO has been synthesised and reported to be electrochemically active. In this work, we perform an extensive computational search for iron-based oxysulphides using *ab initio* random structure searching (AIRSS). By

performing an unbiased sampling of the Li-Fe-S-O chemical space, several oxysulphide phases have been discovered which are predicted to be less than $50\,\mathrm{meV/atom}$ from the convex hull and potentially accessible for synthesis. Among the predicted phases, two anti-Ruddlesden-Popper structured materials $Li_2Fe_2S_2O$ and $Li_4Fe_3S_3O_2$ have been found to be attractive as they have high theoretical capacities with calculated average voltages $2.9\,\mathrm{V}$ and $2.5\,\mathrm{V}$ respectively, and their distances to hull are less than $5\,\mathrm{meV/atom}$. By performing nudged-elastic band calculations, we show that the Li-ion transport in these materials takes place by hopping between the nearest neighbouring sites with low activation barriers between $0.3\,\mathrm{eV}$ and $0.5\,\mathrm{eV}$. The richness of materials yet to be synthesised in the Li-Fe-S-O phase field illustrates the great opportunity in these mixed anion systems for energy storage applications and beyond.

Keywords

1 Introduction

The cathode is a critical component for lithium-ion batteries (LIBs) to achieve high energy density, safe operation, and economical viability. Despite many technological advances in LIBs, the cathode materials have barely evolved in the last 15 years. Those found in commercialised LIBs are still based on one of the three systems: layered $LiCoO_2$,[1] spinel $LiMn_2O_4$[2] and olivine $LiFePO_4$,[3] all of which were first proposed more than two decades ago. Iron-based cathode materials are very attractive as Fe is one of the most abundant transition metal in the upper crust with very low production costs. LIBs with olivine $LiFePO_4$ cathodes are nowadays used in applications including electric vehicles, but they suffer from relatively low specific energies.[4] Other iron based polyanion cathodes, such as Li_2FeSiO_4,[5,6] $LiFeSO_4F$[7–9] have also being proposed and shown to have comparable performance to $LiFePO_4$. The use

of larger-sized polyanion groups, however, places an upper-limit on the energy density, which in turn offsets some of the benefits of the low cost. On the other hand, iron-oxide based cathodes are held back due to low voltages due to the Fe^{2+}/Fe^{3+} redox,[10] while attempts to utilize the Fe^{3+}/Fe^{4+} redox often lead to decomposition into other phases upon charging.[11–13]

Substituting one element with another has been a fruitful strategy for increasing the performance of cathode materials. Over the years, most of the research interests have been focusing on cationic substitution, and materials such as layered $LiNi_xMn_yCo_zO_2$[14] have improved reversible capacities over $LiCoO_2$ - only half of the Li can be extracted in the latter. In the meantime, anionic substitution, or mixed anion materials have been largely unexplored until recently.[15] With different sizes, valence charge, electronegativity and polarizability of the anions, hetero-anionic materials are known to form layered structures due to preferential cation-anion bonding.[16,17] The incorporation of fluorine into oxide has been reported to improve the performance of disordered rock salt type cathodes.[18] It offers another knob for tuning the valence of the transition metal cations and being more electronegative than oxygen leads to higher voltages.[19,20] Anions that are less electronegative can be oxidised more easily than O^{2-}, which could favour anionic redox and leads to higher capacities.[21] For chalcogenide anions (S^{2-} and Se^{2-}), the increased polarizability also gives rise to better electronic conductivity than the oxide and polyanion based materials, which often poses limitations for fast and reversible Li cycling.

Recently, an anti-perovskite structured oxysulphide Li_2FeSO ($Pm\bar{3}m$) was synthesised and found to have reasonably good electrochemical performance with a theoretical cationic redox capacity of 223 mAh/g, and a voltage of 2.5 V against graphite electrodes.[22,23] A subsequent computational study suggests that the anti-perovskite framework provides low lithium-diffusion barriers, and substituting Fe with other transition metal ions could lead to improved performance.[24] Replacing half of the Fe by Mn has been reported to enhanced the structural stability but at the cost of reducing the capacity.[25] Meanwhile, iron oxysulphide based cathodes have also been explored for applications in sodium-ion batteries.[26]

3

These findings beg the question: are there other oxysulphides waiting to be discovered? Computational materials discovery, and in particular, high-throughput screening studies, have previously been applied to many fields including battery cathodes.[27,28] Those studies, however, rely heavily on existing experimental data, as hypothetical materials are constructed from simple substitutions of the known materials.[17,29,30] For lithium iron oxysulphides, which remain largely unexplored so far, the available experimental data are scarce. The other way of discovering new materials is to directly search for low energy structures using first-principles calculations, with little or no experimental inputs.[31] Finding the lowest energy crystal structure is a challenging task, as it requires global optimisation over the high-dimensional configuration space. Many approaches have been developed to tackle the problem, including basin hopping,[32] minima hopping,[33] genetic algorithms[34] and particle-swarm optimisation.[35] In this work, we explore the lithium iron oxysulphide chemical space using *ab initio* random structure searching[36,37] (AIRSS), which is a simple, efficient and highly parallel method for searching for low energy structures. By sampling the Li-Fe-S-O space in an unbiased way, we have discovered many previously unknown phases that are both predicted to be relatively stable and have good electrochemical performances for cathode applications. Among those phases, two anti-Ruddlesden-Popper structured materials $Li_2Fe_2S_2O$ and $Li_4Fe_3S_3O_2$ are particularly attractive due to them being both nearly on the convex hull and have theoretical capacities exceeding that of the Li_2FeSO. Subsequent DFT calculations using the predicted crystal structures show that they have average voltages of $2.9\,V$ and $2.5\,V$ respectively, and band gaps about $2.0\,eV$. Using the climbing-image nudged elastic band method,[38,39] we show that both of them contain Li-diffusion networks with low transition state barriers similar to that of Li_2FeSO.

2 Methods

Details about *ab initio* random structure searching (AIRSS) and its application to battery electrode materials can be found in the literature.[36,37,40,41] Briefly, this method searches for low energy structures by generating random but physically sensible initial structures followed by geometry optimisation using first-principles calculations. Unlike most other structure prediction methods, there is no iterative improvement process involved, hence the search can be parallelized and distributed over the computing resources easily. The plane wave density functional theory code CASTEP[42] is used for structure searching with a plane wave cut off energy of $340\,eV$ and a k-point spacing of $0.07\,2\pi\text{Å}^{-1}$ for sampling the reciprocal space. Core-corrected on-the-fly generated ultrasoft pseudopotentials from CASTEP's built-in QC5 library are used. Further DFT calculations are performed using the VASP[43,44] code with a plane wave cut off energy of $520\,eV$ and a k-point spacing of $0.04\,2\pi\text{Å}^{-1}$. The PBE exchange-correlation functional[45] is used with the Hubbard correction applied for the d states of Fe. The U value for Fe is set to $4.0\,eV$ based on the fitting of oxide formation energies.[46] A force-based convergence criteria of $0.03\,eV\,\text{Å}^{-1}$ is used for all geometry optimisations, except when relaxing the input structure for phonon calculations where a tighter tolerance of $0.0001\,eV\,\text{Å}^{-1}$ is applied. Ferromagnetic spin states have been assumed during the initial search to avoid complicating the energy landscapes. Enumerating spin arrangements for selected low energy phases shows that imposing anti-ferromagnetic orderings typically reduces the energy by 10 to $20\,meV$ per atom, giving minor changes to the computed thermodynamic stabilities. Hence, the FM ordering is used in all further calculations for oxysulphides. Finite-displacement phonon calculations are performed using the Phonopy package[47] with an increased cut off energy of $650\,eV$. Climbing-image nudged elastic band[38,39] calculations are performed for determining the Li-diffusion barriers using the VTST code. The supercells are constructed such that periodic images of the Li-vacancy are more than 10 Å away in all directions. To avoid hole localisation upon creating a single Li vacancy, which would otherwise complicate the potential energy surface and the

minimum energy pathway, a single electron is added to the supercell with a neutralising background. This resembles the case where the polaron formed is far away from the Li-vacancy. The AiiDA framework is used to automate the DFT calculations and preserve their provenance.[48,49] The sumo[50] python package is used for plotting electronic density of states and phonon band structures.
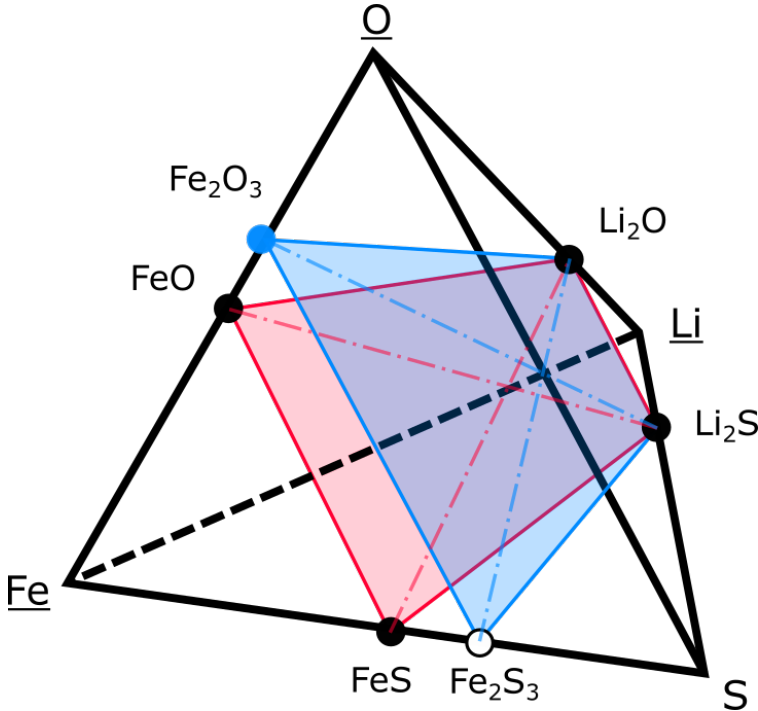
3   Results

New phases in the Li-Fe-O-S space

Figure 1: A tetrahedron representing the Li-Fe-S-O chemical space. charge-neutral compositions with formal valences (Fe: +2/+3, Li: +1, S: -2, O: -2) for oxysulphides are located on the two planes with Fe in +3 (red) and +2 (blue) states.

We target our search for fully lithiated phases of potential materials for Li-intercalation cathodes. The Li-Fe-O-S chemical space can be represented as a tetrahedron with vertices being the elemental species, as shown in Fig. 1. In oxysulphides, both oxygen and sulphur typically have the −2 oxidation states. For metal cations, Li is expected to be in the +1
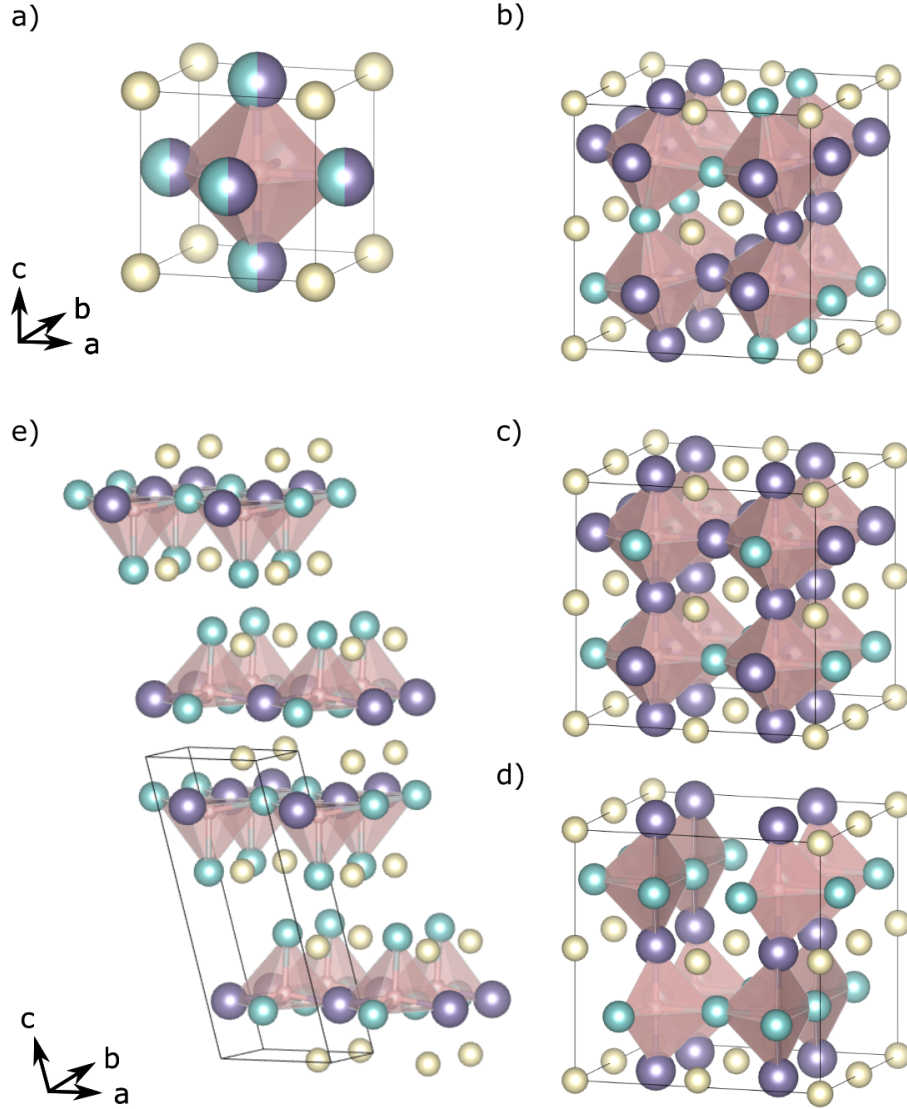
Figure 2: (a) The disordered cubic anti-perovskite unit cell of Li_2FeSO. (b) The Li_2FeSO structure found here. (c) The lowest energy Li_2FeSO reported previously.[24] (d) The structure of $Li_2Fe_3S_2O_2$. (e) The structure of $Li_2Fe_4S_3O_2$. Colour coding: cream-S, purple-Li, cyan-Fe, pink-O.The coordination polyhedrons drawn are centered on oxygen atoms.

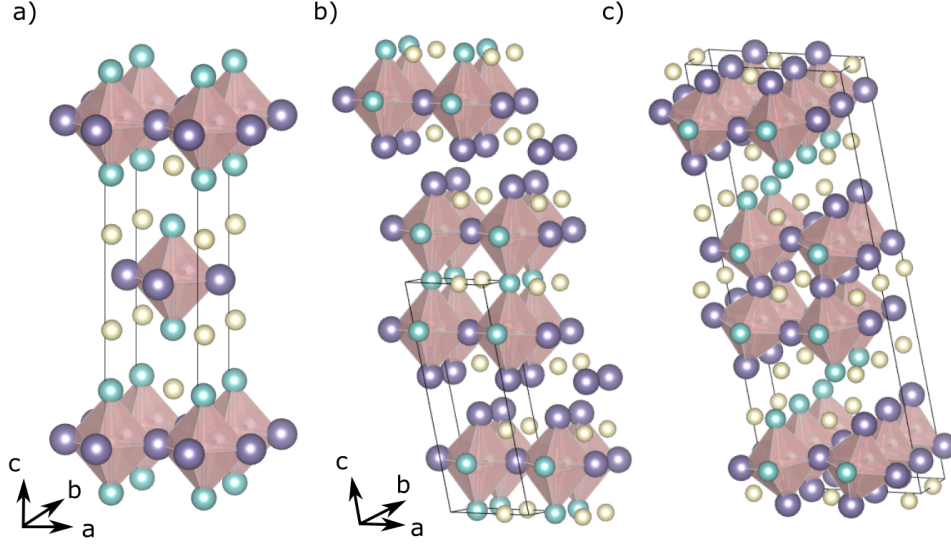Figure 3: The two anti-Ruddlesden-Popper phases found in the search: (a) $Li_2Fe_2S_2O$; (b) $Li_4Fe_3S_3O_2$; (c) $Li_4Fe_3S_3O_2$ with lower energy obtained by enumerating the Li/Fe orderings. Colour coding: cream-S, purple-Li, cyan-Fe, pink-O.The coordination polyhedrons drawn are centered on oxygen atoms.

state and we limit Fe to be in the $+2$ and $+3$ states. To maintain charge neutrality, the sum of the oxidation states for a given composition should be zero. This means that the compositions to be searched are located on two cross-sectional planes of the full Li-Fe-S-O tetrahedron: one for those with Fe in $+3$ and the other for $+2$, as shown in Fig. 1. Plane wave density functional theory calculations are known to have cubic scaling, to keep the problem tractable, we limit the search to compositions with the number of atoms in the empirical formula ≤ 12, and the total number of atoms in the full formula ≤ 24. Even with these constrains applied, there are still 33 candidate compositions to be searched. As a result, we have to perform coarse samplings of the phase space initially, where about 600 random structures generated and relaxed for each composition. Afterwards, compositions that have the lowest energy structure close to the convex are selected for further searching.

The compositions of the phases that are found to be close to the convex hull within a $50\,\text{meV}$ per atom range is shown in Table 1, where V_a is calculated average voltage, ΔV is the volume change after delithiation and E_h is the distance to the convex hull, S_c is the

Table 1: Compositions that are close to the convex hull found in the search and their computed average voltages and theoretical capacities. Symbols: V_a is calculated average voltage; ΔV is the volume change after delithiation; E_h is the distance to the convex hull; S_c is the specific capacity; S_e is the specific energy. The $Li_4Fe_3S_3O_2$ structure obtained from enumeration is marked with the asterisk.

Formula	V_a (V)	ΔV (%)	E_h (meV)	S_c (mAh/g)	S_e (Wh/kg)	Decomposition
Li_2FeSO	2.33	-4.5	0.0	227.5	532.3	N/A
$Li_2Fe_4S_3O_2$	2.72	-7.3	0.0	146.7	398.5	N/A
$Li_4Fe_3S_3O_2{}^*$	2.56	-5.3	3.3	248.6	637.8	$Li_2FeSO + Li_2Fe_4S_3O_2 + Li_2S$
$Li_2Fe_3S_2O_2$	2.56	-10.0	3.4	193.1	496.0	$Li_2FeSO + FeO + Li_2Fe_4S_3O_2$
$Li_2Fe_2S_2O$	2.85	-11.7	3.4	260.6	743.6	$Li_2Fe_4S_3O_2 + Li_2S$
$Li_4Fe_3S_3O_2$	2.55	-3.4	18.1	248.6	633.6	$Li_2FeSO + Li_2Fe_4S_3O_2 + Li_2S$
$Li_4Fe_3S_4O$	2.47	-3.8	30.5	236.8	585.4	$Li_2Fe_4S_3O_2 + FeS + Li_2S$
$Li_2Fe_4S_4O$	2.58	-6.9	38.6	140.5	363.4	$Li_2Fe_4S_3O_2 + FeS + Li_2S$
$Li_4Fe_2S_3O$	2.09	-5.5	45.8	213.0	445.5	$Li_2Fe_4S_3O_2 + Li_2S$
Li_6FeSO_3	1.90	-10.0	46.3	150.9	287.3	$Li_2O + Li_2FeO_2 + Li_2S$
$Li_2Fe_3S_3O$	2.44	-7.6	48.8	182.6	446.5	$Li_2Fe_4S_3O_2 + FeS + Li_2S$
Li_6FeS_3O	2.28	1.5	49.9	127.8	291.5	$Li_2FeSO + Li_2S$

theoretical specific capacity, and S_e is the specific energy computed from on V_a and S_c. The 50 meV distance to hull threshold is chosen because experimentally synthesisable metastable compounds are expected to fall into this range.[51] Our search has also reproduced the anti-perovskite Li_2FeSO phase (Fig. 2a) that was reported previously,[22] and it is predicted to be on the convex hull (e.g. thermodynamically stable) at 0 K. A previous DFT study predicts Li_2FeSO to be metastable and would decompose into Li_2FeO_2, FeS and Li_2S,[24] whereas it is found to be stable here. This difference is likely to be caused by the methodology of treating transition metals in different type of compounds. In that work, the PBE/PBE+U calculations are mixed,[52] where the Hubbard-correction for Fe is only applied to oxide/oxysulphide phases with the energies adjusted using the correction factors from the Materials Project.[28] In this approach, the PBE+U correction factor is supposed to be calibrated for reproducing oxide formation energies involving metallic Fe and O_2. Applying the same term to oxysulphides would introduce systematic errors and affection the reaction energy of forming oxysulphides from oxide and sulphides. We also find that the standard PBE calculations give

large energy differences between polymorphs of FeS and overly destabilise the troilite phase ($P\bar{6}2c$) for which the experimental thermochemical data is available. More discussion can be found in the supporting information. In this work, the Hubbard correction is applied to all Fe-containing phases including the sulphides (similar to that in the Open Quantum Material Database[53]). In theory, the U_{eff} calibrated based on oxide formation energies differs from those for sulphides.[54] Nevertheless, as the distance to hull are computed using the same set of competing phases, phases that are predicted to be close/on the convex hull should have stabilities similar to that of the Li_2FeSO, which has been synthesised experimentally.[22]

The Li_2FeSO structure found by the search here (Fig. 2b, space group Pc) contains Li and Fe atoms with substantial displacements from their sites in the cubic disordered anti-perovskite cell (Fig. 2a, space group $Pm\bar{3}m$). This result can be easily rationalised by invoking our knowledge of perovskite tilting, as the O, Li, and Fe atoms have sizes such that the OLi_4Fe_2 network contains tilted octahedra in the $a^0b^0c^+$ pattern using the Glazer's rotation,[55] which is consistent the Goldschmidt tolerance factor of 0.85 computed from the ionic radii. This value is computed using a weighted average of Li and Fe radii and the ionic radius of S^{2-} in six-fold coordination. The latter may result in underestimation of the tolerance factor as S^{2-} is in fact under 12-fold coordination in the anti-perovskite structure. The previously reported theoretical ground state structure of Li_2FeSO, which was obtained by enumerating Li and Fe sites (shown in Fig. 2c, space group $P4_2mmc$), does not have any octahedral tilting,[24] and it is $6\,meV$ higher in energy compared to our structure obtained using AIRSS. This high-symmetry structure is dynamically unstable (Fig. S4a), and following the imaginary mode at the M point results in $a^-b^-c^0$ tilted octahedra (space group $P2/c$), shown in Fig. S4b. The final energy of this distorted structure is almost identical to the one found with AIRSS. Oxysulphides containing Fe^{3+} are mostly unstable and far from the hull, and all of the phases in Table 1 contain Fe^{2+} instead. This may be attributed to Fe_2O_3 being very stable as one of the competing phases.

Several previously unknown phases have been found to be on or close to the convex

hull. The $Li_2Fe_4S_3O_2$ (space group $C2$) and $Li_2Fe_3S_2O_2$ (space group Pm) are shown in Fig. 2d&e respectively. The former is on the convex hull while the latter is only $3\,meV$ (per atom) above it. They can be regarded as cation deficient variants of anti-Ruddlesden-Popper and anti-perovskite structures. In both cases, the oxygen atoms are under square pyramidal coordination by two Li atoms and three Fe atoms, rather than the octahedral coordination in original archetypes. The cation deficiency can be attributed to the reduced Li-to-Fe ratio. Since a Fe^{2+} cation carries more positive charges, fewer cations are needed to balance the negative charge of the anions. Unfortunately, the lower Li-to-Fe ratios result in reduced specific capacities, making them less attractive as cathode materials.

On the other hand, two anti-Ruddlesden-Popper phases, $Li_2Fe_2S_2O$ and $Li_4Fe_3S_3O_2$, have been found to be close to the convex hull and more promising for cathode applications with specific capacity higher than that of the Li_2FeSO. The former has a layered structure as shown in Fig. 3a, which resembles the Ruddlesden-Popper (RP) phases with a general formula $A_{n+1}B_nX_{3n+1}$. The RP series consist of alternating perovskite-like (ABX_3) and rock salt like (AX) environments along the z the direction. The number n indicates the number of complete ABX_3 perovskite layers between the rock salt BX layer. In contrast to normal RP phases, such as $Sr_3Ru_2O_7$, where cations take the A and B sites, here they take the anion X sites instead, and S and O occupy the A and B sites respectively. This gives the anti-Ruddleseden Popper structured oxysulphides a general formula $S_{n+1}O_n(Fe/Li)_{3n+1}$. The $Li_2Fe_2S_2O$ phase (space group Pc) has $n = 1$ with one perovskite layer followed by the rock salt layer as shown in Fig. 3a, and it is only about $3\,meV$ from the convex hull. Likewise, the $Li_4Fe_3S_3O_2$ phase (space group Cm) has two perovskite layers (e.g. $n = 2$) in the unit cell, as shown in Fig. 3b. This phase is slightly less stable with a distance to hull of $18\,meV$ per atom. Different Li/Fe orderings in the primitive cell and supercells of both phases have been enumerated, and twenty structures with the lowest electrostatic energies are further relaxed by DFT for each case. Unlike the cubic perovskite, the base structure of the RP phase is not unique, which can affect the initial rankings based on the electrostatic energies. We used the

experimental structure of Sr_2RuO_4, $Sr_3Ru_2O_7$ and the structures obtained from the search as the initial templates. For $Li_2Fe_2S_2O$, performing the enumeration did not generate any structure with lower energy. In fact, using the ideal Sr_2RuO_4 structure as the template would miss the lowest energy structure that is found in the search. On the other hand, repeating the same procedure for $Li_4FeS_3O_2$ has generated many structures with lower energies by up to $14.8\,meV$ per atom (distance to hull is reduced to $3.3\,meV$). In this case, starting from the ideal structure appears to give better results. The lowest energy structure (space group $C2/m$) contains OLi_4Fe_2 tilted octahedra in a $a^+b^0c^0$ tilt system, as shown in Fig. 3c.

It should be noted that many of the "above-hull" structures are in fact predicted to decompose into phases are that are themselves found by the search, as shown in Table 1. If only the ternary and binary compounds in the Li-Fe-S-O chemical spaces are considered, many of them would be regarded as stable. This highlights the importance of performing a sufficient and unbiased sampling of the target chemical space for reliably predicting the thermodynamic stabilities.

To check the dynamic stability of the predicted structures, finite displacement phonon calculations have been carried out. The predicted Li_2FeSO structure was found to have no imaginary frequencies across the first Brouline zone. The $Li_2Fe_2S_2O$ structure obtained by the search (Fig. 3a) has a highly symmetric perovskite layer as shown in Fig. 4a. However, when we calculate the phonon band structure, it was found to have imaginary frequencies (Fig. 4c). Pushing along the imaginary mode (at $(-0.5, 0.5, 0)$ of the conventional cell) allows us to obtain a structure with tilted OLi_4Fe_2 octahedra in a $a^0b^+c^0$ tilt system with space group $P2_1$ (Fig. 4b). Recomputing the phonon dispersion reveals that the imaginary mode has disappeared, which can be seen in Fig. 4d. The energy per atom is reduced by about $1\,meV$ for this distorted structure. For $Li_4Fe_3S_3O_2$, the lowest energy structure generated by the enumeration of symmetrically inequivalent structures (Fig. 3c) was found to be dynamically stable. Imaginary frequencies have been also found in $Li_2Fe_3S_2O_2$ and $Li_2Fe_4S_3O_2$, which are subsequently eliminated by following the corresponding modes. Their final dy-
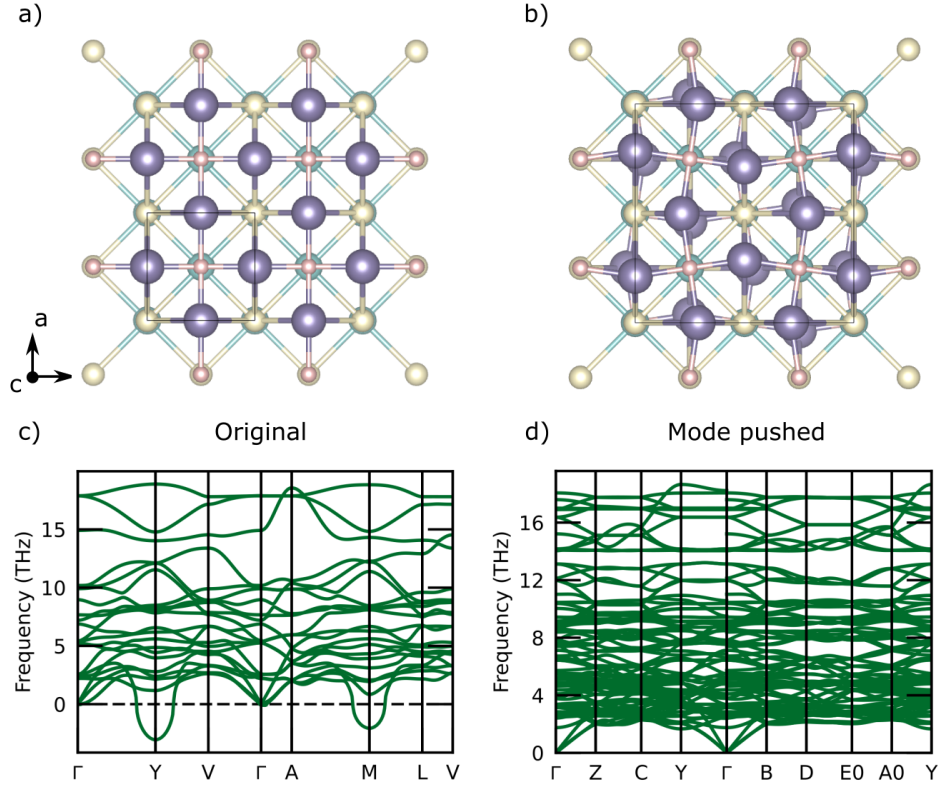
Figure 4: (a) The $Li_2Fe_2S_2O$ from the search, looking down the z direction. (b) The dynamically stable $Li_2Fe_2S_2O$ structure with rotated OLi_4Fe_2 octahedra obtained by following the imaginary phonon modes. (c) The phonon band structure of $Li_2Fe_2S_2O$ with imaginary frequencies. (d) The phonon band structure of mode-pushed $Li_2Fe_2S_2O$. Colour coding: cream-S, purple-Li, cyan-Fe, pink-O.

namically stable structures have lower energies by 2.6 meV and 0.2 meV compared with the non-distorted structures respectively, giving negligible effects on their thermodynamic stabilities. Since the structure searching was carried out with small unit cells containing symmetry operations, distortions that require increased cell sizes are expected to be missing. Nevertheless, as the typically energy reduction after mode-pushing is small, the structures obtained directly from the search are already sufficiently accurate for evaluating thermodynamic stability. Phonon band structures for the phases mentioned above can be be found in the supporting information Fig. S4 and Fig. S5.

Electrochemical properties of the predicted phases

The average voltages, volume changes after delithiation and calculated theoretical capacities of the predicted phases are tabulated in Table 1. For Li-rich phases, only the capacity from the Fe^{2+}/Fe^{3+} redox is considered here, and Li orderings in the delithiated structures are enumerated for calculating the voltages. Li_2FeSO is found to have a voltage of 2.3 V, which is in reasonable agreement with the experimentally obtained 2.5 V. We note that for disordered materials, voltages calculated using small ordered unit cell may not be accurate, and more rigorous approaches such as cluster expansion should provide better results. The two anti-RP phases, $Li_2Fe_2S_2O$ and $Li_4Fe_3S_3O_2$, are predicted to have voltages 2.9 V and 2.5 V respectively. Compared to the Li_2FeSO phase (223 mAh/g), they have higher theoretical capacities (261 mAh/g and 249 mAh/g) because their Li:Fe ratios are closer to 1:1. The voltage profiles of both materials are computed by enumerating unique configurations with different numbers of Li atoms removed in the primitive cells, including four and two formula units respectively. For both $Li_2Fe_2S_2O$ and $Li_4Fe_3S_3O_2$, multiple intermediate phases are found to exists, giving a sloped voltage profile as shown in Fig 5.

The band gaps of the predicted phases are found be to range between 1.8 eV and 2.2 eV using the HSE06 functional, which are a lot narrower than that of $LiFePO_4$, which has a band gap of 3.8 eV - 4.0 eV measured experimentally.[56] In comparison, the band gap of
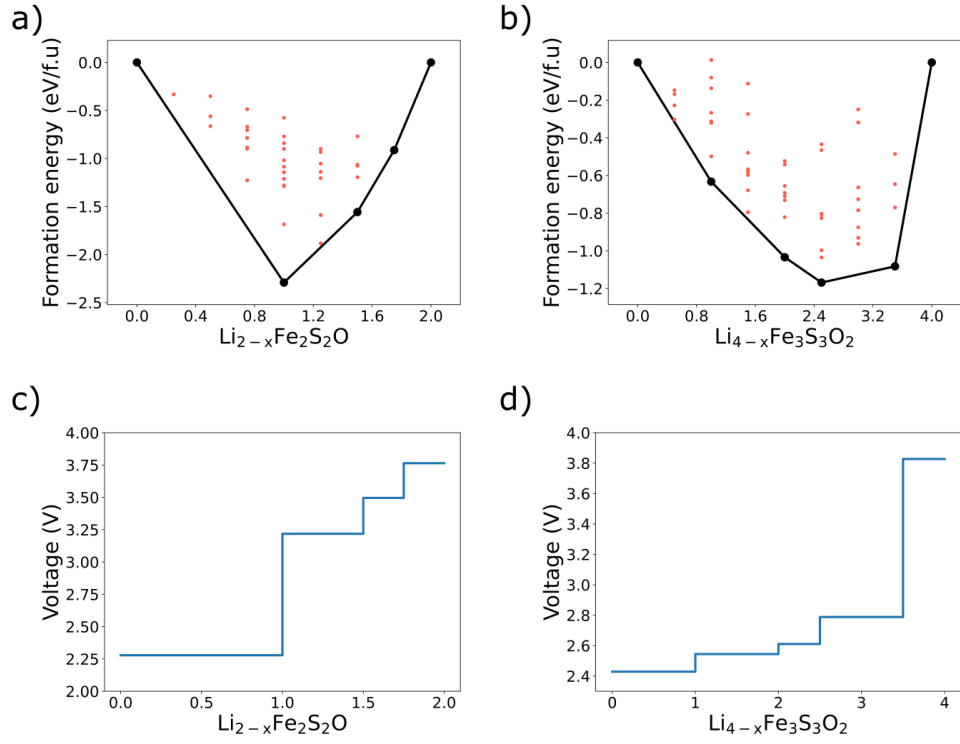
14

Figure 5: Convex hulls of delithiated structures and voltage profiles for (a,c) $Li_2Fe_2S_2O$ and (b, d) $Li_4Fe_3S_2O_2$.

LiCoO$_2$ has been reported to range from 1.7 eV to 2.7 eV in experimental studies.[57,58] Hence, the new oxysulphide phases have the potential of being sufficiently electronically conductive as cathodes. The projected density of states of the predicted phases (Fig. S6) suggest that their valence band maxima are mainly composed of Fe d states with some contributions from oxygen and sulphur p states. This confirms that the Fe^{2+}/Fe^{3+} is the main contributor to the redox capacity.
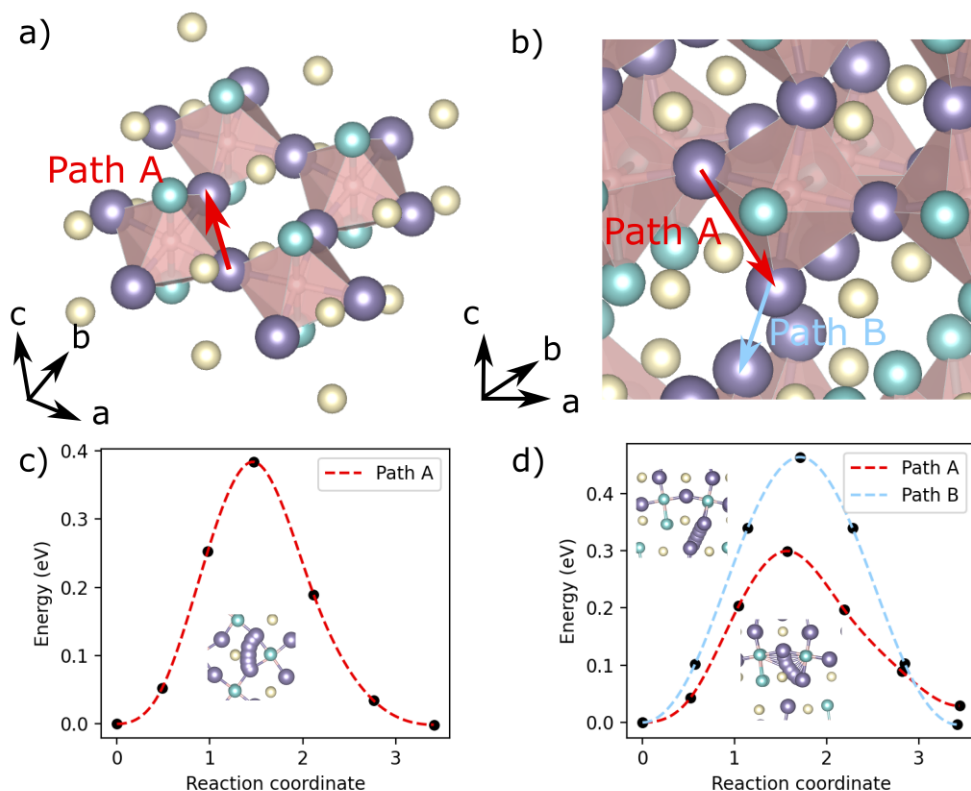

Figure 6: Potential Li diffusion pathways for (a) Li$_2$Fe$_2$S$_2$O (showing only the perovskite layer) and (b) Li$_4$Fe$_3$S$_3$O$_2$ with their corresponding transition state energies (c,d) calculated using the climbing-image nudged elastic band method. Colour coding: cream-S, purple-Li, cyan-Fe, pink-O.The coordination polyhedrons drawn are centered on oxygen atoms.

In addition to good electronic conductivity, the existence of fast lithium ion conduction pathways is also crucial for cathode materials. For Li$_2$Fe$_2$S$_2$O, the Li atoms only occupy the sites within the Li$_2$O layer of the perovskite environment as shown in Fig. 6a. Each Li is under octahedral coordination by four S atoms and two O atoms, and it has four nearest neighbour Li atoms and four next-nearest neighbours. The nearest neighbour pathway is

labelled as Path A in Fig. 6a. The climbing-image nudged elastic band (NEB) method has been use to study the minimum energy pathway for a single Li vacancy to migrate. The barrier between the nearest neighbour (NN) sites is found to be 0.38 eV, as shown in Fig. 6c. Multiple symmetrically equivalent routes like this form a percolating network, allowing Li diffusion in the ab plane shown in Fig 6a. For the next-nearest neighbour (NNN), the barrier height it is increased to 0.95 eV (Fig S7a). The large difference in the barrier heights between the two cases can be understood as the former requires the Li atom to go through the face of the coordination octahedron around it, whereas the latter needs to go squeeze through the edge made of two S atoms with additional repulsion from the nearby Li atoms. In layered cathode materials, the Li atoms are known to take an indirect route though the tetragonal sites going though the faces of LiO_6 octahedra, rather than the direct path though the edges.[59]

The $Li_4Fe_3S_3O_2$ structure has many inequivalent pathways, and we select representative paths in both the perovskite layer and the rock salt layer, as shown in Fig. 6b. The A and B paths corresponds to the NN pathways inside the perovskite and rock salt layers, and they have transitions state barriers 0.30 eV and 0.46 eV respectively. We have also considered the potential pathway though the tetrahedral site coordinated by four S^{2-} in analogy to the diffusion in layered Li metal oxides. However, the Li atom is found to be not stable at that intermediate site, since after relaxations the Li atom returns to its starting position. This can be understood as the occupation of the tetrahedral site would in fact result in very short Li-Fe separation with the Fe atom in the perovskite ordered layer above/below, giving rise to increased electrostatic energies. Here, the direct oxygen-dumbbell hop of Path B is already much lower than the counterpart in $LiCoO_2$,[59] which can be attributed to larger and more polarizable S^{2-} compared with O^{-2}. Similar to $Li_2Fe_2S_2O$, hopping between the NNN sites is found to have much higher barrier heights. The two pathways calculated, Path C and Path D (Fig S7b), are found to have barrier heights of 1.65 eV and 0.94 eV respectively. Within the rock salt layer, Path B forms a percolating channel along the b direction in Fig 6b. A

percolating network also exists in the perovskite layers, which consists of multiple Path A-like segments, permitting the diffusion in both a and c directions. Tilted OFe_2O_4 octahedra result in six inequivalent NN pathways inside the perovskite layer (Fig S7e). To have a more comprehensive coverage of different environments, two more A-like hoping paths are computed, A1 and A2, and found to have barrier heights of 0.40 eV and 0.48 eV respectively (Fig S7c&d). Without exhaustively repeating NEB calculations for all pathways inside the perovskite layer, it is reasonable to conclude that the barrier heights should ranges from 0.3 to 0.5 eV, which are sufficiently low to allow Li diffusion.

4   Discussion

Our computational exploration of the lithium iron oxysulphides has reproduced the known Li_2FeSO phase and a series of other stable and metastable polymorphs, among which the $Li_2Fe_2S_2O$ and $Li_4Fe_3S_2O_2$ have been identified as potential cathode materials. Compositions that are not included in Table 1 are too thermodynamically unstable to be synthesised. Hence they are not investigated further.

The renewed interests in $LiFePO_4$ and advancement in manufacturing processes have made it the top pick for low-cost and sustainable Li-ion batteries. Compared to polyanion based materials, the oxysulphides have the advantage of increased specific capacities. For example, the theoretical capacity of $Li_2Fe_2S_2O$, 260 mAh/g, is much higher than that of the $LiFePO_4$ (170 mAh/g). On the other hand, $LiFePO_4$ has a higher voltage at 3.5 V, giving a theoretical energy density of 595 Wh/kg, while oxysulphides suffer from relatively low voltages (< 3 V). The theoretical energy densities of $Li_2Fe_2S_2O$ (2.9 V) and $Li_4Fe_3S_2O_2$ (2.5 V) are 744 Wh/kg and 633 Wh/kg respectively, which still offer up to 20% increase. Note that due to the poor electrical conductivity of pristine $LiFePO_4$, carbon coating on nanometer-sized particles is necessary to achieve good electrical conductivity,[4,60] which lowers the specific capacity in practice. In comparison, the oxysulphides do not have this problem as they

are expected to have better electric conductivity. Another difference between $LiFePO_4$ and the oxysulphides is that the existence of intermediate delithiated phases in the latter gives sloped voltage curves similar to other oxides based cathodes, whereas the Li intercalation in the former takes place via two-phase reactions, resulting a flat voltage profile.[4]

The distances to hull of the $Li_2Fe_2S_2O$ and $Li_4Fe_3S_3O_2$ (3.4 meV and 3.3 meV) fall into range of the metastability of known quaternary compounds.[51] Nevertheless, having a small distance to hull is not a sufficient condition to infer that experimental synthesis would be straightforward for realising these metastable phases. As our calculations are limited to crystalline phases at $0 \, K$, the effect of disordering is not accounted for. Due to the similar ionic radii of Li^+ and Fe^{2+}, it is possible that the predicted compounds exist in disordered forms. Such entropy contributions from a disordered lattice provide further stabilisation at elevated temperatures. However, this also implies that the competing effect from a disordered Li_2FeSO phase is underestimated in our calculations. Li_2FeSO is found to be stable in calculations, which is not fully consistent with the observed partial decomposition into binary phases at intermediate temperatures.[22] This may be attributed to systematic errors in the treatment of transition metals. Effects of finite-temperature on the free energy is also difficult to include directly in theoretical calculations. We use a recently developed machined learned descriptor to estimate the Gibbs free energy and construct convex hulls at finite temperatures,[61] and the results are found to be qualitatively similar to those computed at $0 \, K$. More details can be found in the supporting information. It is likely that direct synthesis of these predicted phases is no easier than that for Li_2FeSO. Adopting indirect routes may be fruitful. For example, ion-exchange can be a potential approach of synthesising $Li_2FeS_2O_2$ from $Na_2Fe_2S_2O_2$.[26]

5   Conclusion

The Li-Fe-O-S chemical spaces have been explored using ab initio random structure searching (AIRSS), and a series of potentially synthesisable phases that are close to or on the convex hull have been predicted. Among these candidate phases, two anti-RP structures materials $Li_2Fe_2S_2O$ and $Li_4Fe_3S_3O_2$ are particularly promising for cathode applications. Density functional theory calculations show that they have voltages similar to that of the previously reported Li_2FeSO phase, and their theoretical specific capacities exceeds the latter. Fast Li conduction channels are revealed using climbing-image nudged elastic band calculations. If successfully synthesised, they can be good contenders to the commercialised $LiFePO_4$ cathodes. Even though the low voltages (2.9 V and 2.5 V) are nowhere near that of of $LiFePO_4$, they are compensated by much increased theoretical gravimetric capacities ($\sim$250 mAh/g vs $\sim$170 mAh/g). Our work also demonstrates that first-principles structure prediction is an effective way to explore complex quaternary chemical spaces where many new materials are waiting to be discovered for battery cathode applications and beyond.

Supporting Information Available

Supporting Information: Detailed comparisons about correction schemes used for formation energies; Discussion on applying a machined learned descriptor for predicting finite-temperature stability; Figures of phonon band structures and electronic projected density of states of the predicted phases; Additional minimum energy pathway plots of Li-diffusion for $Li_2Fe_2S_2O$ and $Li_4Fe_3S_3O_2$; A link for accessing the calculation data online.

Acknowledgement

References

(1) Mizushima, K.; Jones, P. C.; Wiseman, P. J.; Goodenough, J. B. LixCoO2 (0. *Materials Research Bulletin* **1980**, *15*, 783–789.

(2) Thackeray, M. M.; David, W. I. F.; Bruce, P. G.; Goodenough, J. B. Lithium Insertion into Manganese Spinels. *Materials Research Bulletin* **1983**, *18*, 461–472.

(3) Padhi, A. K.; Nanjundaswamy, K. S.; Goodenough, J. B. Phospho-olivines as Positive-Electrode Materials for Rechargeable Lithium Batteries. *Journal of the Electrochemical Society* **1997**, *144*, 1188.

(4) Huang, H.; Yin, S.-C.; Nazar, L. F. Approaching Theoretical Capacity of LiFePO4 at Room Temperature at High Rates. *Electrochemical and Solid-State Letters* **2001**, *4*, A170.

(5) Nytén, A.; Abouimrane, A.; Armand, M.; Gustafsson, T.; Thomas, J. O. Electrochemical Performance of Li2FeSiO4 as a New Li-Battery Cathode Material. *Electrochemistry Communications* **2005**, *7*, 156–160.

(6) Sirisopanaporn, C.; Masquelier, C.; Bruce, P. G.; Armstrong, A. R.; Dominko, R. Dependence of Li2FeSiO4 Electrochemistry on Structure. *Journal of the American Chemical Society* **2011**, *133*, 1263–1265.

(7) Barpanda, P.; Chotard, J.-N.; Recham, N.; Delacourt, C.; Ati, M.; Dupont, L.; Armand, M.; Tarascon, J.-M. Structural, Transport, and Electrochemical Investigation of Novel AMSO4F (A = Na, Li; M = Fe, Co, Ni, Mn) Metal Fluorosulphates Prepared Using Low Temperature Synthesis Routes. *Inorganic Chemistry* **2010**, *49*, 7401–7413.

(8) Recham, N.; Chotard, J.-N.; Dupont, L.; Delacourt, C.; Walker, W.; Armand, M.; Tarascon, J.-M. A 3.6 V Lithium-Based Fluorosulphate Insertion Positive Electrode for Lithium-Ion Batteries. *Nature Materials* **2010**, *9*, 68–74.

(9) Barpanda, P.; Ati, M.; Melot, B. C.; Rousse, G.; Chotard, J.-N.; Doublet, M.-L.; Sougrati, M. T.; Corr, S. A.; Jumas, J.-C.; Tarascon, J.-M. A 3.90 V Iron-Based Fluorosulphate Material for Lithium-Ion Batteries Crystallizing in the Triplite Structure. *Nature Materials* **2011**, *10*, 772–779.

(10) Morzilli, S.; Scrosati, B. Iron Oxide Electrodes in Lithium Organic Electrolyte Rechargeable Batteries. *Electrochimica Acta* **1985**, *30*, 1271–1276.

(11) Kim, J.; Manthiram, A. Synthesis and Lithium Intercalation Properties of Nanocrystalline Lithium Iron Oxides. *Journal of The Electrochemical Society* **1999**, *146*, 4371.

(12) Matsumura, T.; Kanno, R.; Inaba, Y.; Kawamoto, Y.; Takano, M. Synthesis, Structure, and Electrochemical Properties of a New Cathode Material, LiFeO2 , with a Tunnel Structure. *Journal of The Electrochemical Society* **2002**, *149*, A1509.

(13) Armstrong, A. R.; Tee, D. W.; La Mantia, F.; Novák, P.; Bruce, P. G. Synthesis of Tetrahedral LiFeO2 and Its Behavior as a Cathode in Rechargeable Lithium Batteries. *Journal of the American Chemical Society* **2008**, *130*, 3554–3559.

(14) Kim, J.; Lee, H.; Cha, H.; Yoon, M.; Park, M.; Cho, J. Prospect and Reality of Ni-Rich Cathode for Commercialization. *Advanced Energy Materials* **2018**, *8*, 1702028.

(15) Lee, J.; Papp, J. K.; Clément, R. J.; Sallis, S.; Kwon, D.-H.; Shi, T.; Yang, W.; Mc-Closkey, B. D.; Ceder, G. Mitigating Oxygen Loss to Improve the Cycling Performance of High Capacity Cation-Disordered Cathode Materials. *Nature Communications* **2017**, *8*, 981.

(16) Clarke, S. J.; Denis, S. G.; Rutt, O. J.; Hill, T. L.; Hayward, M. A.; Hyett, G.; Gál, Z. A. Sodium Intercalation into the n = 2 Ruddlesden-Popper Type Host Y2Ti2O5S2: Synthesis, Structure, and Properties of α-NaxY2Ti2O5S2 (0 < x ≤ 1). *Chemistry of Materials* **2003**, *15*, 5065–5072.

(17) Charles, N.; Saballos, R. J.; Rondinelli, J. M. Structural Diversity from Anion Order in Heteroanionic Materials. *Chemistry of Materials* **2018**, *30*, 3528–3537.

(18) Lun, Z.; Ouyang, B.; Cai, Z.; Clément, R. J.; Kwon, D.-H.; Huang, J.; Papp, J. K.; Balasubramanian, M.; Tian, Y.; McCloskey, B. D.; Ji, H.; Kim, H.; Kitchaev, D. A.; Ceder, G. Design Principles for High-Capacity Mn-Based Cation-Disordered Rocksalt Cathodes. *Chem* **2020**, *6*, 153–168.

(19) Deng, D. Transition Metal Oxyfluorides for Next-Generation Rechargeable Batteries. *ChemNanoMat* **2017**, *3*, 146–159.

(20) A. House, R.; Jin, L.; Maitra, U.; Tsuruta, K.; W. Somerville, J.; P. Förstermann, D.; Massel, F.; Duda, L.; R. Roberts, M.; G. Bruce, P. Lithium Manganese Oxyfluoride as a New Cathode Material Exhibiting Oxygen Redox. *Energy & Environmental Science* **2018**, *11*, 926–932.

(21) Saha, S.; Assat, G.; Sougrati, M. T.; Foix, D.; Li, H.; Vergnet, J.; Turi, S.; Ha, Y.; Yang, W.; Cabana, J.; Rousse, G.; Abakumov, A. M.; Tarascon, J.-M. Exploring the Bottlenecks of Anionic Redox in Li-Rich Layered Sulfides. *Nature Energy* **2019**, *4*, 977–987.

(22) Lai, K. T.; Antonyshyn, I.; Prots, Y.; Valldor, M. Anti-Perovskite Li-Battery Cathode Materials. *Journal of the American Chemical Society* **2017**, *139*, 9645–9649.

(23) Lai, K. T.; Antonyshyn, I.; Prots, Y.; Valldor, M. Extended Chemical Flexibility of Cubic Anti-Perovskite Lithium Battery Cathode Materials. *Inorganic Chemistry* **2018**, *57*, 13296–13299.

(24) Lu, Z.; Ciucci, F. Anti-Perovskite Cathodes for Lithium Batteries. *Journal of Materials Chemistry A* **2018**, *6*, 5185–5192.

(25) Gorbunov, M. V.; Carrocci, S.; Maletti, S.; Valldor, M.; Doert, T.; Hampel, S.; Gonzalez Martinez, I. G.; Mikhailova, D.; Gräßler, N. Synthesis of (Li2Fe1–yMny)SO Antiperovskites with Comprehensive Investigations of (Li2Fe0.5Mn0.5)SO as Cathode in Li-Ion Batteries. *Inorganic Chemistry* **2020**, *59*, 15626–15635.

(26) Gamon, J.; Perez, A. J.; Jones, L. A. H.; Zanella, M.; Daniels, L. M.; Morris, R. E.; Tang, C. C.; Veal, T. D.; Hardwick, L. J.; Dyer, M. S.; Claridge, J. B.; Rosseinsky, M. J. Na2Fe2OS2, a New Earth Abundant Oxysulphide Cathode Material for Na-Ion Batteries. *Journal of Materials Chemistry A* **2020**, *8*, 20553–20569.

(27) Ceder, G. Opportunities and Challenges for First-Principles Materials Design and Applications to Li Battery Materials. *MRS Bulletin* **2010**, *35*, 693–701.

(28) Jain, A.; Ong, S. P.; Hautier, G.; Chen, W.; Richards, W. D.; Dacek, S.; Cholia, S.; Gunter, D.; Skinner, D.; Ceder, G.; Persson, K. A. Commentary: The Materials Project: A Materials Genome Approach to Accelerating Materials Innovation. *APL Materials* **2013**, *1*, 011002.

(29) Hautier, G.; Fischer, C.; Ehrlacher, V.; Jain, A.; Ceder, G. Data Mined Ionic Substitutions for the Discovery of New Compounds. *Inorganic Chemistry* **2011**, *50*, 656–663.

(30) Mueller, T.; Hautier, G.; Jain, A.; Ceder, G. Evaluation of Tavorite-Structured Cathode Materials for Lithium-Ion Batteries Using High-Throughput Computing. *Chemistry of Materials* **2011**, *23*, 3854–3862.

(31) Oganov, A. R.; Pickard, C. J.; Zhu, Q.; Needs, R. J. Structure Prediction Drives Materials Discovery. *Nature Reviews Materials* **2019**, *4*, 331.

(32) Wales, D. J.; Doye, J. P. K. Global Optimization by Basin-Hopping and the Lowest Energy Structures of Lennard-Jones Clusters Containing up to 110 Atoms. *The Journal of Physical Chemistry A* **1997**, *101*, 5111–5116.

(33) Goedecker, S. Minima Hopping: An Efficient Search Method for the Global Minimum of the Potential Energy Surface of Complex Molecular Systems. *The Journal of Chemical Physics* **2004**, *120*, 9911–9917.

(34) Oganov, A. R.; Glass, C. W. Crystal Structure Prediction Using Ab Initio Evolutionary Techniques: Principles and Applications. *The Journal of Chemical Physics* **2006**, *124*, 244704.

(35) Wang, Y.; Lv, J.; Zhu, L.; Ma, Y. CALYPSO: A Method for Crystal Structure Prediction. *Computer Physics Communications* **2012**, *183*, 2063–2070.

(36) Pickard, C. J.; Needs, R. J. High-Pressure Phases of Silane. *Physical Review Letters* **2006**, *97*, 045504.

(37) Pickard, C. J.; Needs, R. J. Ab Initio Random Structure Searching. *Journal of physics. Condensed matter : an Institute of Physics journal* **2011**, *23*, 053201–053201.

(38) Henkelman, G.; Uberuaga, B. P.; Jónsson, H. A Climbing Image Nudged Elastic Band Method for Finding Saddle Points and Minimum Energy Paths. *The Journal of Chemical Physics* **2000**, *113*, 9901–9904.

(39) Henkelman, G.; Jónsson, H. Improved Tangent Estimate in the Nudged Elastic Band Method for Finding Minimum Energy Paths and Saddle Points. *The Journal of Chemical Physics* **2000**, *113*, 9978–9985.

(40) Lu, Z.; Zhu, B.; Shires, B. W. B.; Scanlon, D. O.; Pickard, C. J. Ab Initio Random Structure Searching for Battery Cathode Materials. *The Journal of Chemical Physics* **2021**, *154*, 174111.

(41) Harper, A. F.; Evans, M. L.; Morris, A. J. Computational Investigation of Copper Phosphides as Conversion Anodes for Lithium-Ion Batteries. *Chemistry of Materials* **2020**, *32*, 6629–6639.

(42) Clark, S. J.; Segall, M. D.; Pickard, C. J.; Hasnip, P. J.; Probert, M. I. J.; Refson, K.; Payne, M. C. First Principles Methods Using CASTEP. *Zeitschrift für Kristallographie* **2005**, *220*, 567–570.

(43) Kresse, G.; Furthmüller, J. Efficient Iterative Schemes for Ab Initio Total-Energy Calculations Using a Plane-Wave Basis Set. *Physical Review B* **1996**, *54*, 11169–11186.

(44) Kresse, G.; Furthmüller, J. Efficiency of Ab-Initio Total Energy Calculations for Metals and Semiconductors Using a Plane-Wave Basis Set. *Computational Materials Science* **1996**, *6*, 15–50.

(45) Perdew, J. P.; Burke, K.; Ernzerhof, M. Generalized Gradient Approximation Made Simple. *Physical Review Letters* **1996**, *77*, 3865–3868.

(46) Wang, L.; Maxisch, T.; Ceder, G. Oxidation Energies of Transition Metal Oxides within the GGA+U Framework. *Physical Review B* **2006**, *73*, 195107.

(47) Togo, A.; Tanaka, I. First Principles Phonon Calculations in Materials Science. *Scripta Materialia* **2015**, *108*, 1–5.

(48) Huber, S. P.; Zoupanos, S.; Uhrin, M.; Talirz, L.; Kahle, L.; Häuselmann, R.; Gresch, D.; Müller, T.; Yakutovich, A. V.; Andersen, C. W.; Ramirez, F. F.; Adorf, C. S.; Gargiulo, F.; Kumbhar, S.; Passaro, E.; Johnston, C.; Merkys, A.; Cepellotti, A.; Mounet, N.; Marzari, N.; Kozinsky, B.; Pizzi, G. AiiDA 1.0, a Scalable Computational Infrastructure for Automated Reproducible Workflows and Data Provenance. *Scientific Data* **2020**, *7*, 300.

(49) Uhrin, M.; Huber, S. P.; Yu, J.; Marzari, N.; Pizzi, G. Workflows in AiiDA: Engineering a High-Throughput, Event-Based Engine for Robust and Modular Computational Workflows. *Computational Materials Science* **2021**, *187*, 110086.

(50) Ganose, A. M.; Jackson, A. J.; Scanlon, D. O. Sumo: Command-Line Tools for Plotting and Analysis of Periodic *ab Initio* Calculations. *Journal of Open Source Software* **2018**, *3*, 717.

(51) Sun, W.; Dacek, S. T.; Ong, S. P.; Hautier, G.; Jain, A.; Richards, W. D.; Gamst, A. C.; Persson, K. A.; Ceder, G. The Thermodynamic Scale of Inorganic Crystalline Metastability. *Science Advances* **2016**, *2*, e1600225.

(52) Jain, A.; Hautier, G.; Ong, S. P.; Moore, C. J.; Fischer, C. C.; Persson, K. A.; Ceder, G. Formation Enthalpies by Mixing GGA and GGA + U Calculations. *Physical Review B* **2011**, *84*, 045115.

(53) Kirklin, S.; Saal, J. E.; Meredig, B.; Thompson, A.; Doak, J. W.; Aykol, M.; Rühl, S.; Wolverton, C. The Open Quantum Materials Database (OQMD): Assessing the Accuracy of DFT Formation Energies. *npj Computational Materials* **2015**, *1*, 1–15.

(54) Yu, Y.; Aykol, M.; Wolverton, C. Reaction Thermochemistry of Metal Sulfides with GGA and $\mathrm{GGA}+U$ Calculations. *Physical Review B* **2015**, *92*, 195118.

(55) Glazer, A. M. The Classification of Tilted Octahedra in Perovskites. *Acta Crystallo-*

graphica Section B: Structural Crystallography and Crystal Chemistry **1972**, *28*, 3384–3392.

(56) Zhou, F.; Kang, K.; Maxisch, T.; Ceder, G.; Morgan, D. The Electronic Structure and Band Gap of LiFePO4 and LiMnPO4. *Solid State Communications* **2004**, *132*, 181–186.

(57) Kushida, K.; Kuriyama, K. Narrowing of the Co-3d Band Related to the Order–Disorder Phase Transition in LiCoO2. *Solid State Communications* **2002**, *123*, 349–352.

(58) Ensling, D.; Thissen, A.; Laubach, S.; Schmidt, P. C.; Jaegermann, W. Electronic Structure of ${\text{LiCoO}}_{2}$ Thin Films: A Combined Photoemission Spectroscopy and Density Functional Theory Study. *Physical Review B* **2010**, *82*, 195431.

(59) Van der Ven, A.; Ceder, G. Lithium Diffusion Mechanisms in Layered Intercalation Compounds. *Journal of Power Sources* **2001**, *97-98*, 529–531.

(60) Bewlay, S. L.; Konstantinov, K.; Wang, G. X.; Dou, S. X.; Liu, H. K. Conductivity Improvements to Spray-Produced LiFePO4 by Addition of a Carbon Source. *Materials Letters* **2004**, *58*, 1788–1791.

(61) Bartel, C. J.; Millican, S. L.; Deml, A. M.; Rumptz, J. R.; Tumas, W.; Weimer, A. W.; Lany, S.; Stevanović, V.; Musgrave, C. B.; Holder, A. M. Physical Descriptor for the Gibbs Energy of Inorganic Crystalline Solids and Temperature-Dependent Materials Chemistry. *Nature Communications* **2018**, *9*, 4168.

TOC Graphic